Pragmatic Improvement of Magnetic Exchange Couplings from Subsystem Density-Functional Theory through Orthogonalization of Subsystem Orbitals
— Supporting Information —

Anja Massolle and Johannes Neugebauer[1]

Theoretische Organische Chemie, Organisch-Chemisches Institut

and Center for Multiscale Theory and Computation,

Westfälische Wilhelms-Universität Münster

Corrensstraße 36, 48149 Münster, Germany

Date: February 16, 2021

---

[1]email: j.neugebauer@uni-muenster.de

S1 Lewis Structures

In Fig. S1 the Lewis formulas of the radical monomers employed in this work are shown.

SAXPOW ITULIT JASKEW DESJET
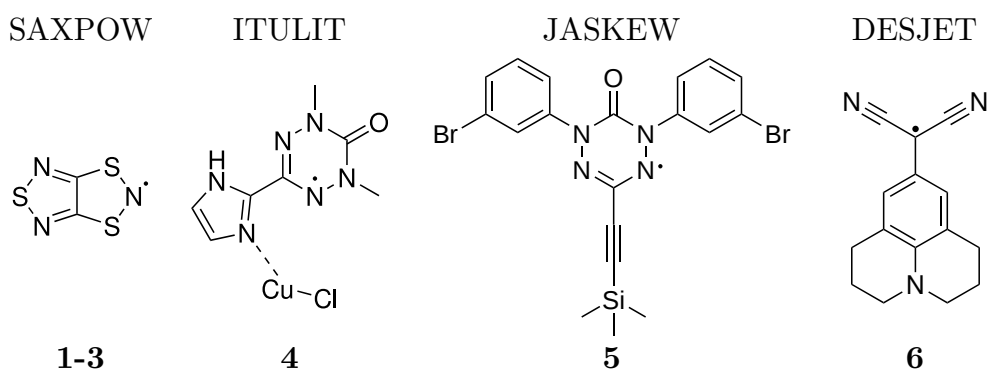
1-3 **4** **5** **6**

Figure S1: Lewis structures of the radical monomers studied in this work. The corresponding CCDC identifier is listed above the Lewis structure.

S2 Density Error Introduced by the Orthogonalization

The integrated spin density error introduced by the Löwdin orthogonalization procedure is shown in Fig S2 to S6 for compounds **2-6**.
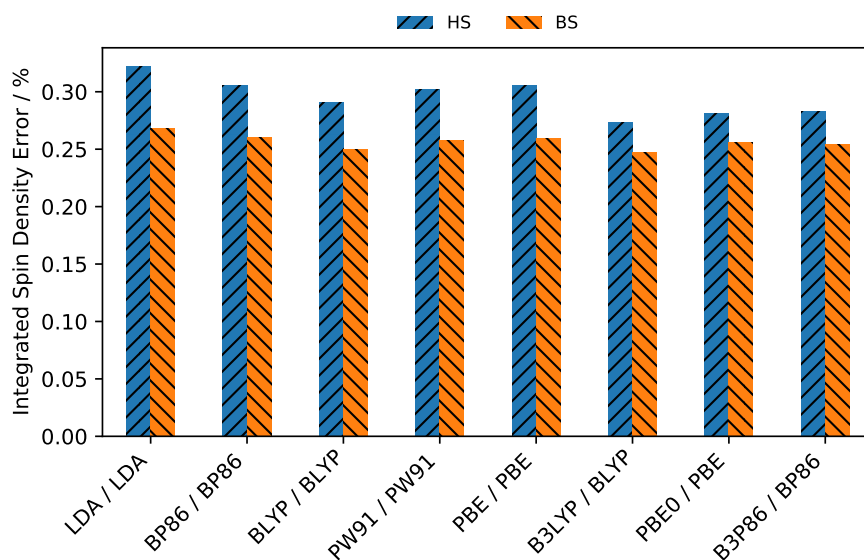

Figure S2: Integrated spin density error for compound **2** after applying the Löwdin orthogonalization. The XC / nad XC functional combination employed in the sDFT calculation is shown on the x axis.

Figure S3: Integrated spin density error for compound **3** after applying the Löwdin orthogonalization. The XC / nad XC functional combination employed in the sDFT calculation is shown on the x axis.
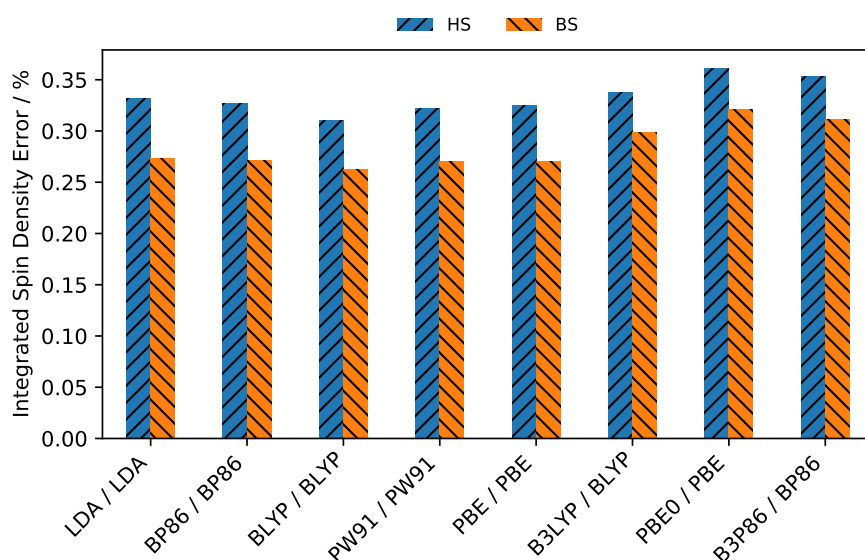
Figure S4: Integrated spin density error for compound **4** after applying the Löwdin orthogonalization. The XC / nad XC functional combination employed in the sDFT calculation is shown on the x axis.
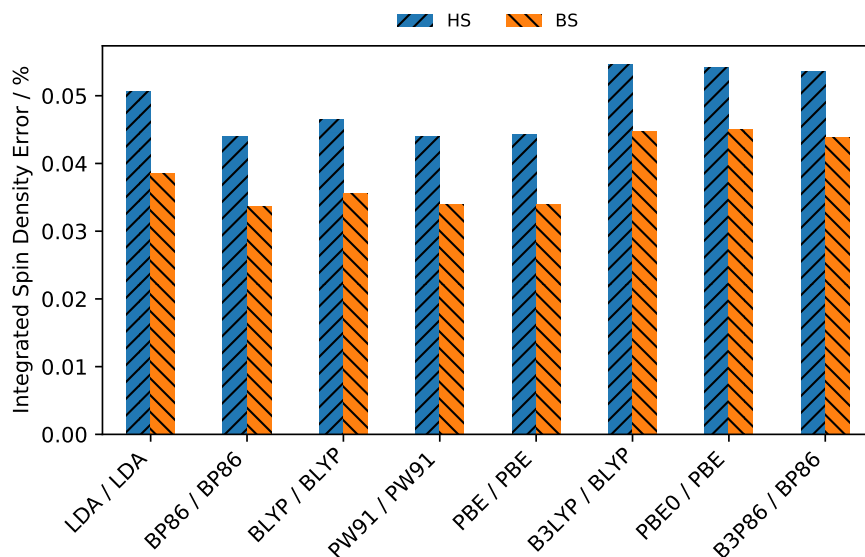
Figure S5: Integrated spin density error for compound **5** after applying the Löwdin orthogonalization. The XC / nad XC functional combination employed in the sDFT calculation is shown on the x axis.

Figure S6: Integrated spin density error for compound **6** after applying the Löwdin orthogonalization. The XC / nad XC functional combination employed in the sDFT calculation is shown on the x axis.
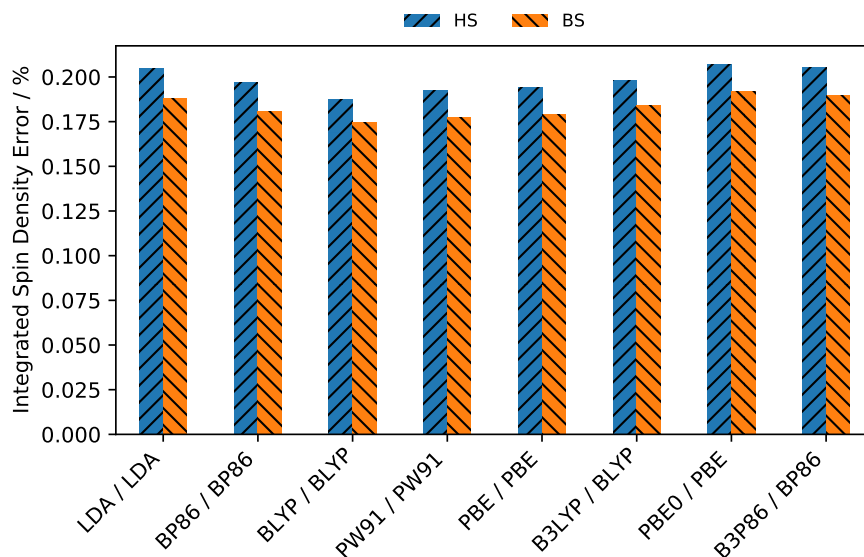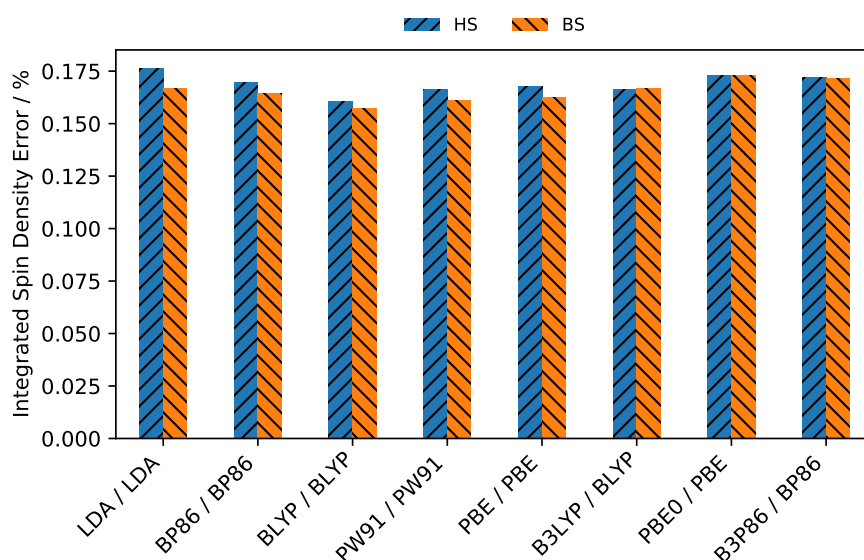
S3 Other Orthogonalization Techniques

To test the numeric stability of different orthogonalization techniques we calculated the magnetic coupling constant J with four different procedures.

Löwdin Löwdins symmetric orthogonalization[1] as described in the main article.

Pipek Pipeks iterative procedure which tries to keep the orbitals as local as possible.[2]

Broer Broers orthogonalization method which is based on corresponding orbitals.[3]

$\mathbf{T}_{\mathbf{kin}}^{\mathbf{non\text{-}ortho}}$ The kinetic energy can also be calculated from non-orthogonal orbitals by expressing the density matrix in the following way:[4]

$$P = CS^{-1}C^{\mathsf{T}}. \tag{S1}$$

The kinetic energy of the supersystem can then be evaluated as:

$$E_{\mathrm{kin}} = \sum_{i,j}^{n_{\mathrm{bas}}} P_{ij} \left\langle \chi_i(\mathbf{r}) \left| -\frac{\nabla^2}{2} \right| \chi_j(\mathbf{r}) \right\rangle \tag{S2}$$

Where $\chi(\mathbf{r})$ are the AO basis functions and P is the density matrix from Eq. (S1).

In Tab. S1 the magnetic exchange coupling constants calculated with method B (only T_s^{nad} is calculated from the orthogonal orbitals) and the four orthogonalization procedures are listed.

Table S1: Mean values and standard deviations of J (in units of cm^{-1}) calculated with the XC-functionals listed in the computational details for all investigated systems. When sDFT was employed T_s^{nad} was either calculated from a NAKE functional or by orthogonalized subsystem orbitals. Method B was employed for the energy evaluation via orthogonalized orbitals.

		1	**2**	**3**	**4**	**5**	**6**
KS-DFT	mean	-1696	-195	-19	-833	-499	-6
	std	199	85	9	216	154	7
sDFT, NAKE	mean	-61	-10	0	-27	-11	-3
	std	4	2	0	3	2	1
sDFT, Löwdin	mean	-2724	-162	-10	-845	-406	-12
	std	46	19	1	168	26	1
sDFT, Pipek	mean	-2724	-162	-10	-845	-406	-12
	std	46	19	1	168	26	1
sDFT, Broer	mean	-2724	-162	-10	-845	-406	-12
	std	46	19	1	168	26	1
sDFT, $T_{\mathrm{kin}}^{\text{non-otho}}$	mean	-2724	-162	-10	-845	-406	-12
	std	46	19	1	168	26	1

S4 Magnetic Exchange Coupling Constants

In Tab. S2 to S6 the magnetic exchange coupling constants calculated for compounds **2-6** with KS-DFT and different sDFT methods are compiled.

Table S2: Magnetic exchange coupling constants (in units of cm^{-1}) evaluated with the PW91k NAKE functional, without any NAKE contribution and via method A and B for Löwdin orthogonalized orbitals for compound **2**.

XC	nad XC	NAKE	$T_s^{\mathrm{nad}} = 0$	Method A (all)	Method B (T_s^{nad})	KS-DFT
LDA	LDA	−6	5	−18	−188	−328
BP86	BP86	−12	−1	−21	−174	−237
BLYP	BLYP	−13	−3	−22	−168	−225
PW91	PW91	−10	0	−20	−172	−230
PBE	PBE	−10	0	−21	−175	−236
B3LYP	BLYP	−11	0	−19	−140	−104
PBE0	PBE	−9	2	−17	−138	−93
B3P86	BP86	−10	2	−18	−143	−105

Table S3: Magnetic exchange coupling constants (in units of cm^{-1}) evaluated with the PW91k NAKE functional, without any NAKE contribution and via method A and B for Löwdin orthogonalized orbitals for compound **3**.

XC	nad XC	NAKE	$T_s^{\mathrm{nad}} = 0$	Method A (all)	Method B (T_s^{nad})	KS-DFT
LDA	LDA	0	0	−2	−12	−33
BP86	BP86	0	0	−2	−11	−23
BLYP	BLYP	0	0	−2	−11	−23
PW91	PW91	0	0	−2	−11	−22
PBE	PBE	0	0	−2	−11	−23
B3LYP	BLYP	0	0	−1	−9	−9
PBE0	PBE	0	0	−1	−8	−7
B3P86	BP86	0	0	−1	−9	−9

Table S4: Magnetic exchange coupling constants (in units of cm^{-1}) evaluated with the PW91k NAKE functional, without any NAKE contribution and via method A and B for Löwdin orthogonalized orbitals for compound **4**.

XC	nad XC	NAKE	$T_s^{nad} = 0$	Method A (all)	Method B (T_s^{nad})	KS-DFT
LDA	LDA	-22	10	-131	-692	-940
BP86	BP86	-26	7	-138	-746	-1106
BLYP	BLYP	-30	1	-139	-729	-1088
PW91	PW91	-25	8	-134	-732	-530
PBE	PBE	-26	7	-135	-723	-548
B3LYP	BLYP	-31	17	-171	-1019	-843
PBE0	PBE	-27	28	-174	-1072	-773
B3P86	BP86	-27	24	-170	-1047	-839

Table S5: Magnetic exchange coupling constants (in units of cm^{-1}) evaluated with the PW91k NAKE functional, without any NAKE contribution and via method A and B for Löwdin orthogonalized orbitals for compound **5**.

XC	nad XC	NAKE	$T_s^{nad} = 0$	Method A (all)	Method B (T_s^{nad})	KS-DFT
LDA	LDA	-7	5	-56	-387	-731
BP86	BP86	-11	1	-59	-394	-584
BLYP	BLYP	-14	-2	-60	-382	-569
PW91	PW91	-11	2	-58	-388	-562
PBE	PBE	-11	2	-57	-390	-571
B3LYP	BLYP	-13	5	-67	-426	-337
PBE0	PBE	-10	10	-68	-444	-305
B3P86	BP86	-11	8	-66	-438	-336

Table S6: Magnetic exchange coupling constants (in units of cm^{-1}) evaluated with the PW91k NAKE functional, without any NAKE contribution and via method A and B for Löwdin orthogonalized orbitals for compound **6**.

XC	nad XC	NAKE	$T_s^{nad} = 0$	Method A (all)	Method B (T_s^{nad})	KS-DFT
LDA	LDA	-1	2	0	-8	-14
BP86	BP86	-3	-1	-3	-12	-10
BLYP	BLYP	-4	-2	-3	-12	-12
PW91	PW91	-3	-1	-2	-11	-10
PBE	PBE	-3	-1	-2	-12	-9
B3LYP	BLYP	-3	-1	-2	-12	1
PBE0	PBE	-2	-1	-1	-12	3
B3P86	BP86	-3	-1	-2	-12	2

The magnetic exchange coupling constants of **1** to **6** calculated with sDFT using the PW91k NAKE functional, orthogonalized orbitals and KS-DFT are depicted in Fig. S7 to S12.
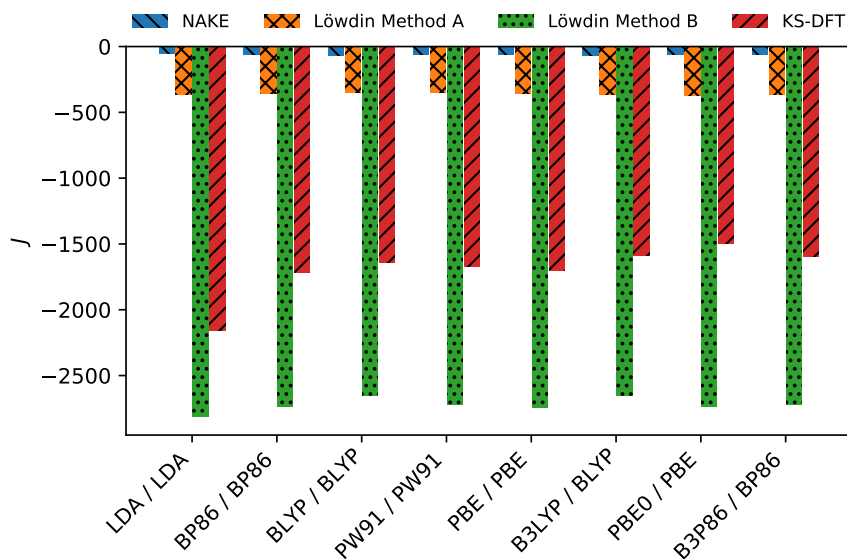

Figure S7: Magnetic exchange coupling constants evaluated for compound **1** with different schemes for the calculation of T_s^{nad} and various XC / nad XC functionals. NAKE: T_s^{nad} evaluated with a NAKE functional and Löwdin: T_s^{nad} evaluated from Löwdin orthogonalized orbitals via method A or B. The corresponding KS-DFT values calculated with the listed XC functional are shown for reference.
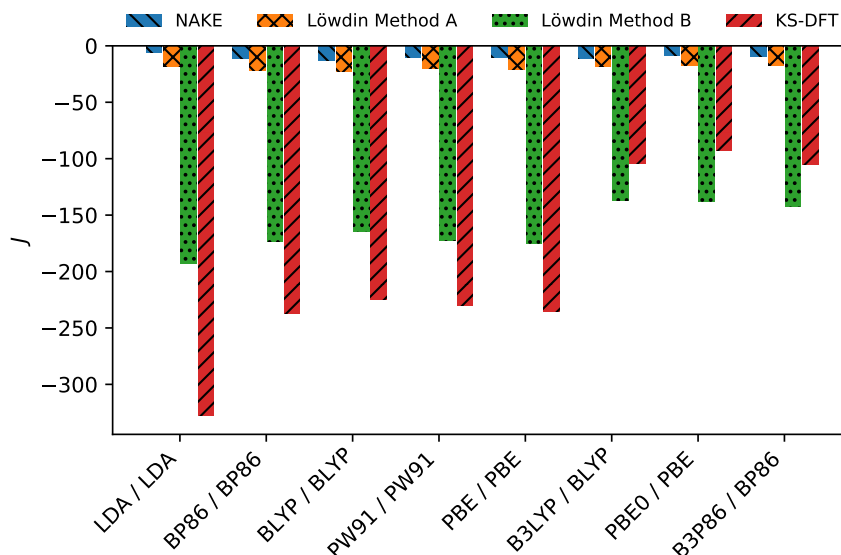
Figure S8: Magnetic exchange coupling constants evaluated for compound **2** with different schemes for the calculation of T_s^{nad} and various XC / nad XC functionals. NAKE: T_s^{nad} evaluated with a NAKE functional and Löwdin: T_s^{nad} evaluated from Löwdin orthogonalized orbitals via method A or B. The corresponding KS-DFT values calculated with the listed XC functional are shown for reference.
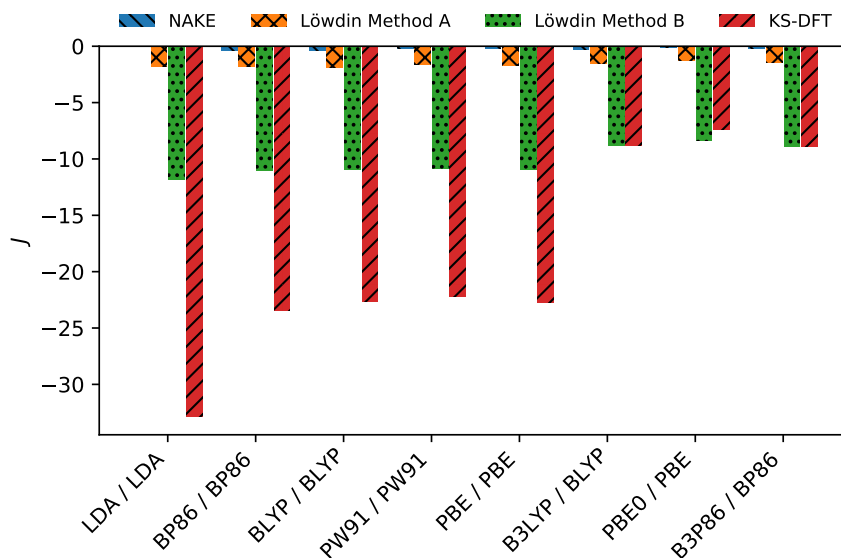

Figure S9: Magnetic exchange coupling constants evaluated for compound **3** with different schemes for the calculation of T_s^{nad} and various XC / nad XC functionals. NAKE: T_s^{nad} evaluated with a NAKE functional and Löwdin: T_s^{nad} evaluated from Löwdin orthogonalized orbitals via method A or B. The corresponding KS-DFT values calculated with the listed XC functional are shown for reference.

Figure S10: Magnetic exchange coupling constants evaluated for compound **4** with different schemes for the calculation of T_s^{nad} and various XC / nad XC functionals. NAKE: T_s^{nad} evaluated with a NAKE functional and Löwdin: T_s^{nad} evaluated from Löwdin orthogonalized orbitals via method A or B. The corresponding KS-DFT values calculated with the listed XC functional are shown for reference.
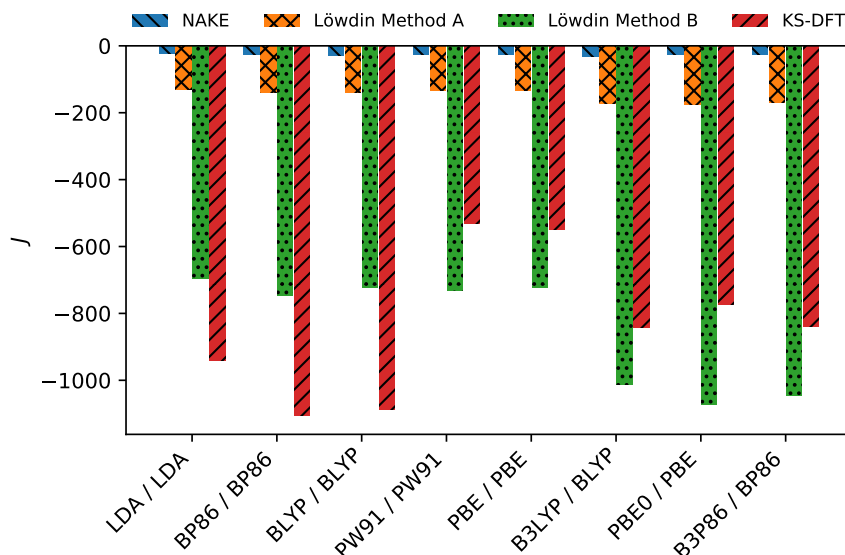

Figure S11: Magnetic exchange coupling constants evaluated for compound **5** with different schemes for the calculation of T_s^{nad} and various XC / nad XC functionals. NAKE: T_s^{nad} evaluated with a NAKE functional and Löwdin: T_s^{nad} evaluated from Löwdin orthogonalized orbitals via method A or B. The corresponding KS-DFT values calculated with the listed XC functional are shown for reference.
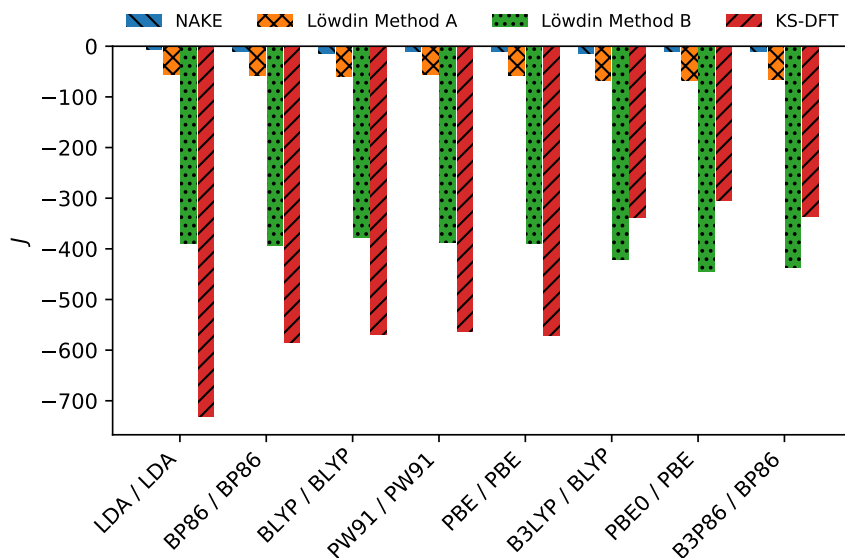
Figure S12: Magnetic exchange coupling constants evaluated for compound **6** with different schemes for the calculation of T_s^{nad} and various XC / nad XC functionals. NAKE: T_s^{nad} evaluated with a NAKE functional and Löwdin: T_s^{nad} evaluated from Löwdin orthogonalized orbitals via method A or B. The corresponding KS-DFT values calculated with the listed XC functional are shown for reference.
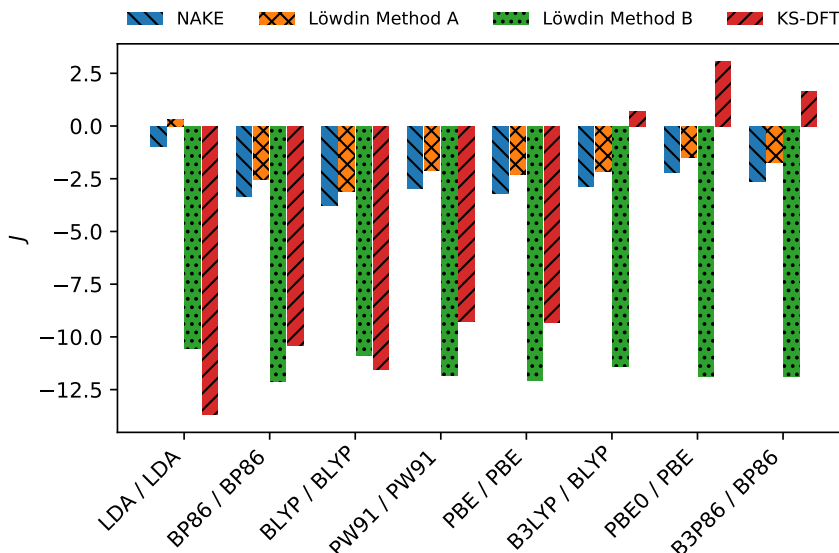
S5 Basis-Set Dependency

To further investigate the basis-set dependency of the sDFT calculations the difference in the spin density introduced by a change of the basis-set is investigated. Figure S13 shows the difference in the spin density introduced by a change of the basis-set from def2-TZVP to def2-SVP. In case of the sDFT and KS-DFT calculations a change in the spin density is visible. The influence of the basis-set on the spin density is large compared to the spin density difference introduced by the orthogonalization procedure, see Fig. 3 in the main article (the isovalue used in Fig. 3 is a power of ten smaller).
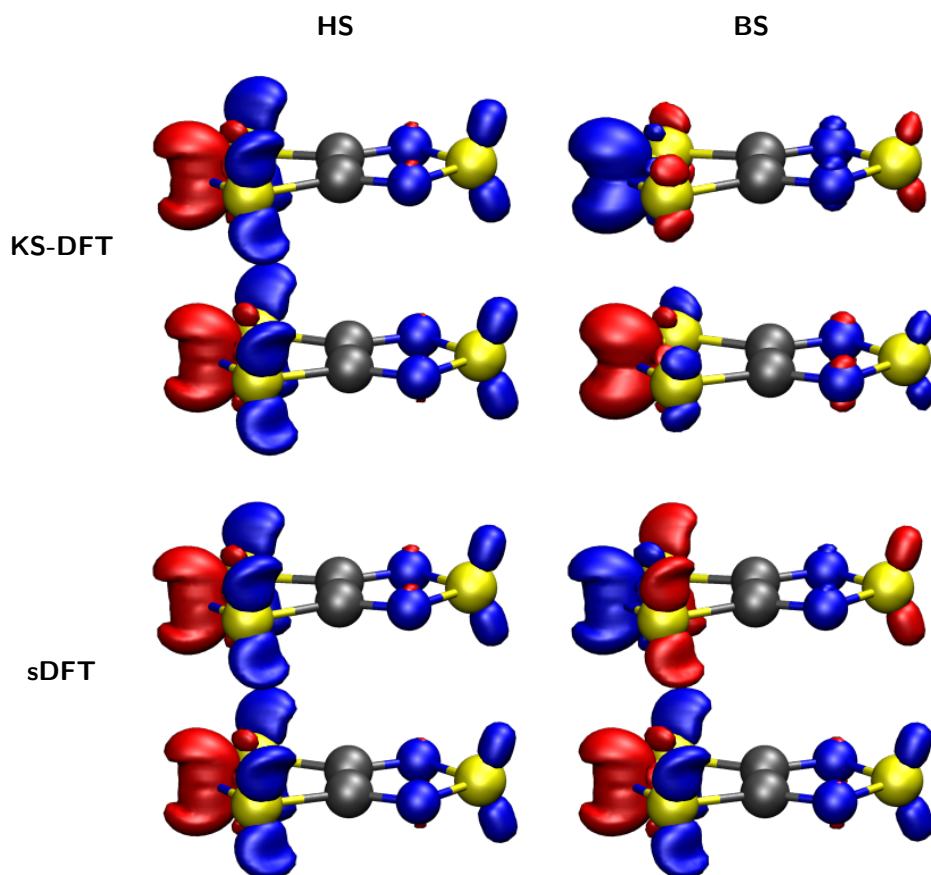
Figure S13: Spin density difference between the def2-TZVP and def2-SVP basis-set of the HS (left) and BS (right) state of dimer **1**. The PBE0/PBE/PW91k functional combination was used for the sDFT calculations (bottom) while the PBE0 XC-functional was employed in the KS-DFT calculations (top). An isovalue of 0.001 E_h was applied.

The magnetic exchange coupling constants shown in Tab. 6 in the main article indicate an increase of the absolute value by about 50% when the def2-TZVP basis-set is used instead of the def2-SVP one. In Tab. S8 to S12 the BS−HS energy differences of the electrostatic, kinetic, XC and total energy contributions are listed for the def2-SVP and def2-TZVP basis-set.

Table S7: Electrostatic, kinetic, XC and total energy differences between the BS and HS state of dimer **1** for the def2-SVP and def2-TZVP basis-set and the PBE0/PBE/PW91k functional combination. All energy differences are given in E_h.

	KS-DFT PBE0	NAKE	Subsystem DFT Pot. Rec. Method A	Method B	Löwdin Method A	Method B
			def2-SVP			
$\Delta E_{\text{electrostatic}}^{\text{BS}-\text{HS}}$	0.081 603	0.002 947	0.007 750	0.002 947	0.012 552	0.002 947
$\Delta E_{\text{kin}}^{\text{BS}-\text{HS}}$	−0.110 161	−0.003 692	−0.013 894	−0.013 894	−0.016 074	−0.016 074
$\Delta E_{\text{XC}}^{\text{BS}-\text{HS}}$	0.020 722	0.000 463	0.000 726	0.000 463	0.001 804	0.000 465
$\mathbf{\Delta E_{total}^{BS-HS}}$	−0.007 836	−0.000 282	−0.005 418	−0.010 484	−0.001 719	−0.012 662
			def2-TZVP			
$\Delta E_{\text{electrostatic}}^{\text{BS}-\text{HS}}$	0.090 488	0.004 135	−0.000 301	0.004 135	0.019 507	0.004 135
$\Delta E_{\text{kin}}^{\text{BS}-\text{HS}}$	−0.125 424	−0.005 599	−0.007 072	−0.007 072	−0.025 186	−0.025 186
$\Delta E_{\text{XC}}^{\text{BS}-\text{HS}}$	0.025 627	0.001 038	0.000 790	0.001 038	0.003 247	0.001 039
$\mathbf{\Delta E_{total}^{BS-HS}}$	−0.009 309	−0.000 427	−0.006 584	−0.001 899	−0.002 432	−0.020 011

Table S8: Electrostatic, kinetic, XC and total energy differences between the BS and HS state of dimer **2** for the def2-SVP and def2-TZVP basis-set and the PBE0/PBE/PW91k functional combination. All energy differences are given in E_h.

	Subsystem DFT NAKE	Method A	Method B
	def2-SVP		
$\Delta E_{\text{electrostatic}}^{\text{BS}-\text{HS}}$	0.000 529	0.001 023	0.000 529
$\Delta E_{\text{kin}}^{\text{BS}-\text{HS}}$	−0.000 657	−0.001 247	−0.001 247
$\Delta E_{\text{XC}}^{\text{BS}-\text{HS}}$	0.000 089	0.000 146	0.000 089
$\mathbf{\Delta E_{total}^{BS-HS}}$	−0.000 040	−0.000 078	−0.000 629
	def2-TZVP		
$\Delta E_{\text{electrostatic}}^{\text{BS}-\text{HS}}$	0.001 003	0.002 453	0.001 003
$\Delta E_{\text{kin}}^{\text{BS}-\text{HS}}$	−0.001 371	−0.003 093	−0.003 093
$\Delta E_{\text{XC}}^{\text{BS}-\text{HS}}$	0.000 294	0.000 472	0.000 293
$\mathbf{\Delta E_{total}^{BS-HS}}$	−0.000 074	−0.000 169	−0.001 797

Table S9: Electrostatic, kinetic, XC and total energy differences between the BS and HS state of dimer **3** for the def2-SVP and def2-TZVP basis-set and the PBE0/PBE/PW91k functional combination. All energy differences are given in E_h.

| | Subsystem DFT | | |
| | NAKE | | |
		Method A	Method B
	def2-SVP		
$\Delta E^{\text{BS}-\text{HS}}_{\text{electrostatic}}$	0.000 009	0.000 035	0.000 009
$\Delta E^{\text{BS}-\text{HS}}_{\text{kin}}$	−0.000 012	−0.000 049	−0.000 049
$\Delta E^{\text{BS}-\text{HS}}_{\text{XC}}$	0.000 003	0.000 008	0.000 003
$\mathbf{\Delta E^{\text{BS}-\text{HS}}_{\text{total}}}$	−0.000 001	−0.000 006	−0.000 038
	def2-TZVP		
$\Delta E^{\text{BS}-\text{HS}}_{\text{electrostatic}}$	−0.000 020	−0.000 015	−0.000 020
$\Delta E^{\text{BS}-\text{HS}}_{\text{kin}}$	0.000 022	0.000 011	0.000 011
$\Delta E^{\text{BS}-\text{HS}}_{\text{XC}}$	0.000 001	0.000 003	0.000 001
$\mathbf{\Delta E^{\text{BS}-\text{HS}}_{\text{total}}}$	0.000 002	−0.000 001	−0.000 009

Table S10: Electrostatic, kinetic, XC and total energy differences between the BS and HS state of dimer **4** for the def2-SVP and def2-TZVP basis-set and the PBE0/PBE/PW91k functional combination. All energy differences are given in E_h.

| | Subsystem DFT | | |
| | NAKE | | |
		Method A	Method B
	def2-SVP		
$\Delta E^{\text{BS}-\text{HS}}_{\text{electrostatic}}$	0.000 883	0.004 310	0.000 883
$\Delta E^{\text{BS}-\text{HS}}_{\text{kin}}$	−0.001 243	−0.006 043	−0.006 043
$\Delta E^{\text{BS}-\text{HS}}_{\text{XC}}$	0.000 238	0.000 933	0.000 241
$\mathbf{\Delta E^{\text{BS}-\text{HS}}_{\text{total}}}$	−0.000 123	−0.000 799	−0.004 919
	def2-TZVP		
$\Delta E^{\text{BS}-\text{HS}}_{\text{electrostatic}}$	0.000 826	0.005 967	0.000 826
$\Delta E^{\text{BS}-\text{HS}}_{\text{kin}}$	−0.001 410	−0.008 459	−0.008 459
$\Delta E^{\text{BS}-\text{HS}}_{\text{XC}}$	0.000 440	0.001 431	0.000 442
$\mathbf{\Delta E^{\text{BS}-\text{HS}}_{\text{total}}}$	−0.000 144	−0.001 060	−0.007 190

Table S11: Electrostatic, kinetic, XC and total energy differences between the BS and HS state of dimer **5** for the def2-SVP and def2-TZVP basis-set and the PBE0/PBE/PW91k functional combination. All energy differences are given in E_h.

	Subsystem DFT NAKE	Method A	Method B
def2-SVP			
$\Delta E_{\text{electrostatic}}^{\text{BS}-\text{HS}}$	0.000 362	0.001 768	0.000 362
$\Delta E_{\text{kin}}^{\text{BS}-\text{HS}}$	−0.000 511	−0.002 496	−0.002 496
$\Delta E_{\text{XC}}^{\text{BS}-\text{HS}}$	0.000 102	0.000 419	0.000 102
$\mathbf{\Delta E_{\text{total}}^{\text{BS}-\text{HS}}}$	−0.000 046	−0.000 309	−0.002 031
def2-TZVP			
$\Delta E_{\text{electrostatic}}^{\text{BS}-\text{HS}}$	0.000 358	0.002 706	0.000 358
$\Delta E_{\text{kin}}^{\text{BS}-\text{HS}}$	−0.000 617	−0.003 818	−0.003 818
$\Delta E_{\text{XC}}^{\text{BS}-\text{HS}}$	0.000 203	0.000 689	0.000 196
$\mathbf{\Delta E_{\text{total}}^{\text{BS}-\text{HS}}}$	−0.000 057	−0.000 422	−0.003 263

Table S12: Electrostatic, kinetic, XC and total energy differences between the BS and HS state of dimer **6** for the def2-SVP and def2-TZVP basis-set and the PBE0/PBE/PW91k functional combination. All energy differences are given in E_h.

	Subsystem DFT NAKE	Method A	Method B
def2-SVP			
$\Delta E_{\text{electrostatic}}^{\text{BS}-\text{HS}}$	0.000 081	0.000 117	0.000 081
$\Delta E_{\text{kin}}^{\text{BS}-\text{HS}}$	−0.000 114	−0.000 158	−0.000 158
$\Delta E_{\text{XC}}^{\text{BS}-\text{HS}}$	0.000 023	0.000 034	0.000 023
$\mathbf{\Delta E_{\text{total}}^{\text{BS}-\text{HS}}}$	−0.000 010	−0.000 007	−0.000 054
def2-TZVP			
$\Delta E_{\text{electrostatic}}^{\text{BS}-\text{HS}}$	0.000 016	−0.000 019	0.000 016
$\Delta E_{\text{kin}}^{\text{BS}-\text{HS}}$	−0.000 034	0.000 013	0.000 013
$\Delta E_{\text{XC}}^{\text{BS}-\text{HS}}$	0.000 020	0.000 011	0.000 018
$\mathbf{\Delta E_{\text{total}}^{\text{BS}-\text{HS}}}$	0.000 002	0.000 005	0.000 047

S6 Geometric Dependency – Orbitals

The heat maps in Fig. 6 in the main article show a sign change of the coupling constant at $\Delta h = 1.8, 2.4$Å and 3.0Å. The SOMO orbitals of the HS and BS state with $\Delta v = 0.0$Å and $\Delta h = 0.0, 1.2, 1.8, 2.4$Å and 3.0Å are shown in Fig. S14.
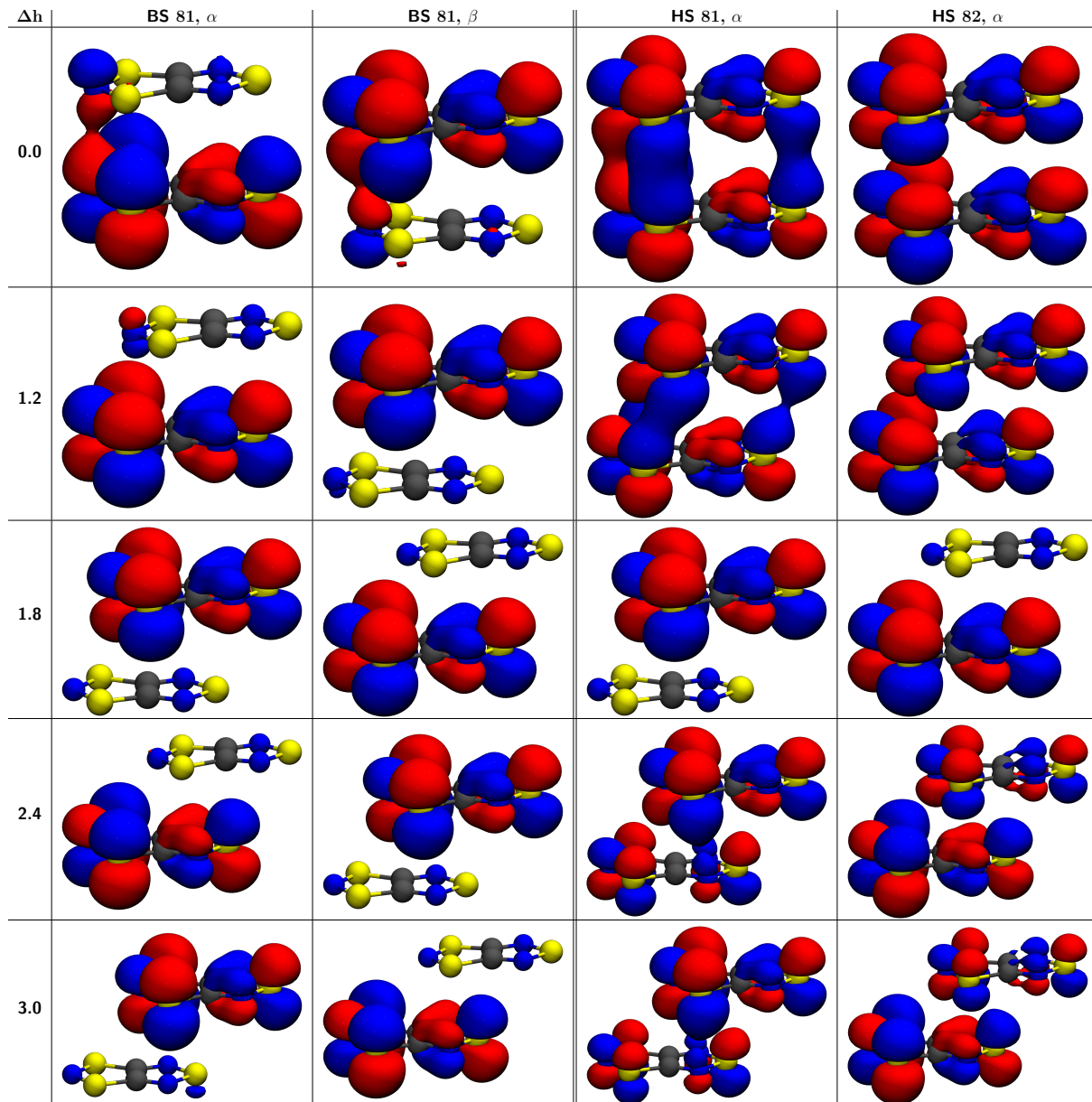

Figure S14: SOMO orbitals of dimer **1** for different Δh and $\Delta v = 0.0$Å calculated with KS-DFT employing the PBE0 XC-functional and def2-SVP basis set for the HS and BS state. An isovalue of 0.025 a.u. was applied.

S7 Interaction Energy

The intermolecular interaction energy was calculated via KS-DFT using the PBE0 XC functional and def2-TZVP basis-set without and with counterpoise correction, see Tab. S13 and Tab. S14. Dimer **1** has the strongest interaction in the HS state.

Table S13: Intermolecular interaction energy of the radical pairs, calculated with PBE0 KS-DFT as $E_{\text{Dimer}} - E_{\text{Monomer 1}} - E_{\text{Monomer 2}}$ employing the def2-TZVP basis-set. The monomer structures are fixed from the dimer structure.

	HS / E_h	BS / E_h
1	0.0156	0.0063
2	0.0015	0.0009
3	−0.0036	−0.0036
4	−0.0016	−0.0057
5	−0.0021	−0.0036
6	−0.0155	−0.0155

Table S14: Intermolecular interaction energy of the radical pairs, calculated with PBE0 KS-DFT as $E_{\text{Dimer}} - E_{\text{Monomer 1}} - E_{\text{Monomer 2}}$. with the def2-TZVP basis-set and counterpoise correction. The monomer structures are fixed from the dimer structure.

	HS / E_h	BS / E_h
1	0.0167	0.0074
2	0.0024	0.0018
3	−0.0030	−0.0030
4	0.0010	−0.0031
5	−0.0004	−0.0019
6	−0.0148	−0.0147

The values in the heat maps shown in Fig. 6 in the main article posses the same values within the reported precision at 1.8 Å, but there are actually small differences as shown in Tab. S15.

Table S15: Geometric dependency of the magnetic exchange coupling constants with $\Delta h = 1.8$ Å, see also Fig. 6 in the main article.

Δv	Δh	KS-DFT	Isolated	FAT
0.2 Å	1.8 Å	7.49 cm^{-1}	7.42 cm^{-1}	6.01 cm^{-1}
0.1 Å	1.8 Å	9.77 cm^{-1}	10.15 cm^{-1}	8.12 cm^{-1}
0.0 Å	1.8 Å	12.51 cm^{-1}	13.19 cm^{-1}	10.54 cm^{-1}
−0.1 Å	1.8 Å	15.72 cm^{-1}	16.31 cm^{-1}	13.15 cm^{-1}
−0.2 Å	1.8 Å	19.16 cm^{-1}	19.08 cm^{-1}	15.36 cm^{-1}

S8 $\langle \mathbf{S^2} \rangle$ Values

The $\langle S^2 \rangle$ values of the HS and BS state for the KS-DFT calculations of compound **6** are shown in Fig. S15.
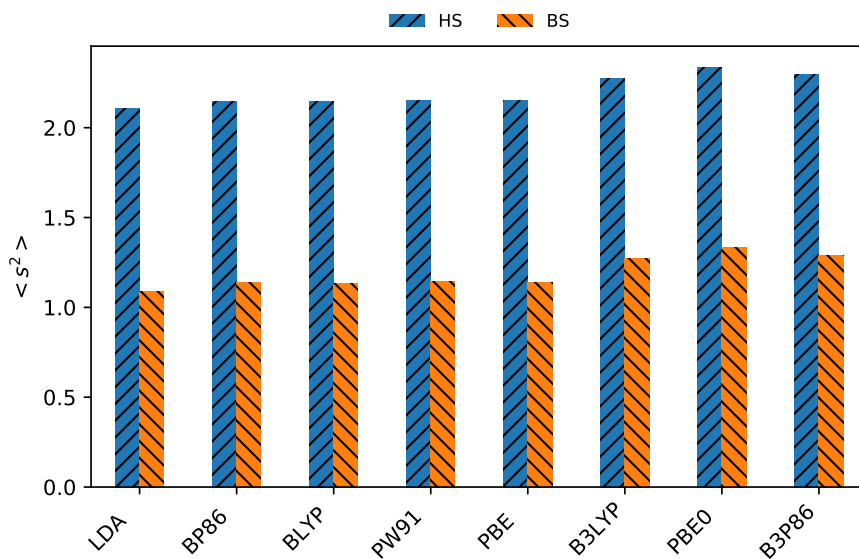

Figure S15: KS-DFT calculated $\langle S \rangle$ values of compound **6** for the HS and BS state.

References

[1] Löwdin, P.-O. On the Non-Orthogonality Problem Connected with the Use of Atomic Wave Functions in the Theory of Molecules and Crystals. *The Journal of Chemical Physics* **1950**, *18*, 365–375.

[2] Pipek, J. Controlled Orthogonalization of Localized Orbitals. *Int. J. Quantum Chem.* **1985**, *27*, 527–546.

[3] Broer, R. On the Use of Corresponding Orbitals for the Construction of Mutually Orthogonal Orbital Sets. *Int. J. Quantum Chem.* **1993**, *45*, 587–590.

[4] Mo, Y.; Peyerimhoff, S. D. Theoretical Analysis of Electronic Delocalization. *J. Chem. Phys.* **1998**, *109*, 1687–1697.